Long non-coding RNA NKILA regulates the JAK2/STAT3 pathway to exacerbate TGF-β1-mediated renal fibrosis

YU HAN[1], SIQI YANG[2,3], JING ZHANG[4], YAOGUANG WANG[5], XI ZHAO[5] and HUAN LIU[5,6]

[1]Department of Nephrology, Tianjin Academy of Traditional Chinese Medicine Affiliated Hospital, Tianjin 300120, P.R. China;
[2]Department of Nephrology, Affiliated Hospital of Nanjing University of Chinese Medicine, Nanjing, Jiangsu 210029, P.R. China;
[3]Department of Nephrology, Jiangsu Province Hospital of Chinese Medicine, Nanjing, Jiangsu 210029, P.R. China;
[4]Department of Hematology, First Teaching Hospital of Tianjin University of Traditional Chinese Medicine, Tianjin 300381, P.R. China;
[5]Department of Nephrology, First Teaching Hospital of Tianjin University of Traditional Chinese Medicine, Tianjin 300381, P.R. China;
[6]Department of Graduate Studies, Tianjin University of Traditional Chinese Medicine, Tianjin 301617, P.R. China

Received August 7, 2025; Accepted january 26, 2026

DOI: 10.3892/mmr.2026.13839

Abstract. Renal interstitial fibrosis is a common pathological outcome of acute and chronic kidney disease. Within the present study, the aim was to explore whether long non-coding RNA (lncRNA) NKILA regulates TGF-β1-induced renal tubular epithelial fibrosis through the JAK-2/STAT3 pathway and its underlying mechanisms. A renal fibrosis model was established by treating HK-2 cells with TGF-β1. RNA sequencing revealed marked dysregulation of the cis-regulated lncRNA NKILA, associated with the JAK2/STAT3 pathway. Functional studies involved overexpressing NKILA using lentivirus in HK-2 cells with TGF-β1-treated cells as a control and knocking it down in the fibrotic model. The JAK2 inhibitor AG490 was employed for rescue experiments. Protein and mRNA levels of epithelial-mesenchymal transition (EMT) markers [fibronectin, collagen I, epithelial (E)-cadherin, α-smooth muscle actin and vimentin] and JAK2/STAT3 pathway components were assessed using western blotting, immunofluorescence and reverse transcription-quantitative PCR. Findings revealed that lncRNA NKILA overexpression promoted fibrosis of TGF-β1-treated HK-2 cells by activating the JAK2/STAT3 pathway. While knockdown of lncRNA NKILA alleviated the TGF-β1-induced EMT damage in HK-2 cells, downregulated EMT markers and upregulated E-cadherin expression by suppressing the activation of the JAK2/STAT3 pathway. Of note, AG490 prevented the damaging effects of lncRNA NKILA or TGF-β1-induced HK-2 cells. Mechanistically, lncRNA NKILA promoted TGF-β1-induced renal injuries by activating the JAK2/STAT pathway. Overall, this suggests that lncRNA NKILA functions as an independent fibrogenic factor and affects the progression of renal interstitial fibrosis by regulating the JAK2/STAT3 signaling pathway.

Correspondence to: Professor Yaoguang Wang, Department of Nephrology, First Teaching Hospital of Tianjin University of Traditional Chinese Medicine, 88 Changling Road, Xiqing, Tianjin 300381, P.R. China
E-mail: wangyaoguang1012@126.com

Key words: long non-coding RNA NKILA, JAK2/STAT pathway, renal interstitial fibrosis

Introduction

Renal interstitial fibrosis (RIF) is the accumulation of scarring within the parenchyma and represents a common final pathway in the majority of chronic and progressive kidney diseases (1). The histopathological characteristics of RIF are extracellular matrix (ECM) component deposition, tubular cell loss, fibroblast aggregation and a sparse peritubular microvascular system (2). The process of ECM deposition in the early stage of tissue injury contributes to the repair of damage, but in the process of chronic kidney disease (CKD), persistent tissue damage will lead to local tissue inflammation. Inflammatory cell-derived free radicals initiate epithelial-mesenchymal transition (EMT), leading to uncontrolled ECM accumulation and accelerated fibrogenesis. This pathological cascade ultimately disrupts organ architecture, impairs perfusion and culminates in functional deterioration, driving progressive CKD toward end-stage renal disease (ESRD) (3-6). Epidemiological data have revealed a marked rise in CKD prevalence, currently affecting 9.1% of the global population. Furthermore, ~50% of these patients will progress to ESRD, substantially compromising their quality of life (7).

Long non-coding RNAs (lncRNAs), typically defined as RNA transcripts >200 nucleotides without protein-coding capacity, exhibit precise spatiotemporal and tissue-specific expression patterns (8-10). These molecules function as key regulators in cellular processes such as cell cycle control, differentiation and metabolic homeostasis. Their regulatory influence extends across multiple tiers of gene expression, encompassing chromatin organization, transcriptional activation and post-transcriptional modifications. Notably, emerging evidence has positioned lncRNAs as upstream master regulators that drive inflammatory responses and orchestrate fibrotic

progression across numerous organ systems, including hepatic, cardiac, pulmonary and renal tissues (11-13).

In the present study, the classical TGF-β1 factor was used to construct an EMT model of HK-2 cells. High-throughput sequencing was used to screen the most significantly differentially expressed lncRNAs in the EMT model, and the downstream molecular mechanisms of the screened results were explored to explore their possible biological functions and their role in the process of RIF.

The lncRNA NKILA, an inflammation-related lncRNA serves a role in numerous disease types, including cardiovascular and cerebrovascular diseases, neuronal diseases, type 2 diabetes, acute kidney injury and immune regulation (14,15). Sequencing results suggest that it may also serve an important role in the process of renal fibrosis. However, at present, understanding of its function is limited. The majority of studies explain the synergistic effect of lncRNA NKILA from the perspective of the synergistic effect of NKILA and NF-κB pathway (16-19), but its complete biological and molecular mechanism has not been fully elucidated. Inflammation is a key process in renal fibrosis and the JAK2/STAT3 signaling pathway is a notable pathway involved in the process of inflammation and fibrosis. Previous studies have shown that lncRNA NKILA has STAT family-associated binding sites in the promoter region (20,21). Therefore, the present study hypothesized that lncRNA NKILA is implicated in renal fibrosis by regulating the JAK2/STAT3 signaling pathway. Subsequently, an *in vitro* cell experiment was designed to validate this hypothesis.

Materials and methods

lncRNA transcriptome sequencing analysis of HK-2 cells induced by TGF-β1. All cells were purchased from Procell Life Science & Technology Co., Ltd. and genotyped at the short tandem repeat and Amelogenin locus. The cell lines used in the present study were all commercial cell lines and did not involve human experimental ethics.

HK-2 cells (cat. no. CL-0109) were cultured in RPMI 1640 medium (cat. no. L220KJ; Shanghai Basal Media Technologies Co., Ltd), supplemented with 10% FBS (cat. no. FBSSR-01021-5, Suzhou Cyagen Biosciences Inc.) at 37˚C in a humified 5% CO_2 atmosphere in a CO_2 incubator. The cells were divided into a normal and a control group. After the cells adhered to 30-40% confluence in a 75 cm^2 flask (cat. no. 430720; Corning, Inc.), the cells were treated with RPMI 1640 medium without FBS for 12 h at 37˚C . The normal group was cultured in RPMI 1640 with FBS for 24 h at 37˚C. In the control group, HK-2 cells were induced using 10 ng/ml TGF-β1 (cat. no. 100-21; PeproTech, Inc; Thermo Fisher Scientific, Inc.) for 24 h at 37˚C to construct the RIF model. Total RNA extraction, quality testing and high-throughput sequencing of lncRNA were performed by Hangzhou Lianchuan Biotechnology Co., Ltd.

Stranded RNA libraries were constructed using ribosomal RNA-depleted RNAs. Libraries were controlled for quality, quantified using a Qubit™ fluorometer (cat. no. Q32857, Thermo Fisher Scientific) and diluted to 1 ng/μl. The RNA integrity was assessed using the Agilent 2100 Bioanalyzer (Agilent Technologies, Inc.) with RNA integrity number >7.0. The final library concentration was 12 nM. The average insert size for the final cDNA library was 300±50 bp. RNA libraries were sequenced using the Illumina NovaSeq™ 6000 (cat. no. 20012850. Illumina, Inc.) with a sequencing read length of 2x150 bp (paired-end 150 bp) at both ends, by 12 cycles. The sequencing depth was 30x and the quantity of data generated was ≥6GB.

Initial data processing involved adapter trimming and quality filtering of raw sequencing reads using Cutadapt (22), eliminating sequences containing adapter contaminants, low-quality bases or undetermined nucleotides. Data processing was performed using the R language R Studio (version 4.1.3; Posit Software, PBC), read quality was assessed with FastQC (Version 0.11.9; bioinformatics.babraham.ac.uk/projects/fastqc/). Alignment to the human reference genome was performed using Bowtie2 (Version 2.4.4) (23) and HISAT2 (Version HISAT-3N beta) (24). Finally, transcript assembly for each sample was performed with StringTie (Version 2.2.0) (25) based on the successfully mapped reads. Subsequently, the transcriptome was assembled using the StringTie program. The expression abundances of mRNAs and lncRNAs were quantified in fragments per kilobase million (FPKM) units utilizing StringTie. Differential expression analysis was performed using the 'edgeR' package (26) in R Studio (version 4.1.3; Posit Software, PBC), with significance thresholds set at log2 (fold change)>1 and adjusted $P<0.05$. After filtering out known mRNA and transcript variants (<200 bp in length), putative lncRNAs were identified by integrating the Coding Potential Calculator (CPC) (27) and the Coding-Non-Coding Index (CNCI) (28). The intersections of non-coding transcripts identified by CNCI and CPC were considered as the putative lncRNAs. Subsequently, the GENCODE database (gencodegenes.org/) was used to were aligned to the reference human genome. The specific transcription factor binding site was predicted by searching the promoter region of NKILA from 2,000 bp upstream to 99 bp downstream using the JASPAR database (29).

The Gene Ontology (GO) database (geneontology.org) was employed for functional annotation of genes. Scatter plots were generated to visualize the top 20 most significantly enriched GO terms (ranked by adjusted P-value). Statistical significance was defined as an adjusted P-value <0.05.

Cell culture, transfection and treatment. HK-2 cells were cultured in RPMI-1640 medium, supplemented with 10% FBS at 37˚C. According to the results of lncRNA microarray analyses, the overexpression (OE) lentivirus (Lv)-NKILA (cat. no. 76304), knockdown (KD) Lv-NKILA-short hairpin (sh)-RNA 1 (cat. no. 108126) and Lv-NKILA-shRNA 2 (cat. no. 108127) vectors were constructed by Genechem. Empty vectors were used as the negative control (NC) groups. Before Lv transfection, HK-2 cells were seeded in 6-well plates at a density of $1x10^4$/ml (1 ml/well), so that the cells were evenly distributed. When the cell density reached 20-30%, Lv transfection was performed according to the multiplicity of infection (MOI), whereby MOI=(virus titer x virus volume)/cell number. Before transfection, fresh complete medium was replaced and the MOI=5 volume Lv solution and 200 μl HiTransGA solution (cat. no. REVG004, GeneChem Inc.) was added for transfection. After virus

transfection, cell proliferation status was observed every 4 h. Furthermore, 10 h after virus transfection, fresh complete medium was replaced and the cells were continually cultured until cell density reached 70-80%. The NC lentiviral vectors (LVCON313, $1x10^9$ TU/ML; LVCON335 was $2.5x10^8$ TU/ML), the oe Lv (Lv-NKILA was $1x10^9$ TU/ML) and the KD Lvs (Lv-NKILA-shRNA 1was $6x10^8$ TU/ml and 2 was $7x10^8$ TU/ml) were transfected into normally cultured HK-2 cells at MOI=5. After transfection, the cells were cultured under in RPMI-1640 medium (cat. no. L220KJ; Shanghai Basal Media Technologies Co., Ltd), supplemented with 10% FBS (cat. no. FBSSR-01021-5, Suzhou Cyagen Biosciences Inc.) at 37˚C, after 10 h virus transfection, the cells were cultured in fresh medium until the cell density was 70-80% and the expression levels of lncRNA NKILA was detected by reverse transcription-quantitative PCR (RT-qPCR) to evaluate the effects of OE and KD. To investigate the role of lncRNA NKILA in RIF, the OE Lv, KD Lv and empty vectors were transfected into HK-2 cells or TGF-β1 induced HK-2 cells with a MOI=5. Following a 10-h transduction period, the medium was replaced with fresh culture medium, and cells were incubated for an additional 24 h until they reached 70-80% confluence. Subsequently, cells were harvested for downstream analyses. The group details were as follows: i) In the normal group, after starvation treatment, HK-2 cells were replaced with fresh complete medium and cultured for an additional 24 h; ii) in the OE-NC group, cells were transfected with a NC virus (LVCON335) and Lv transfection was performed for 24 h at 37˚C; iii) in the control group, 10 ng/ml TGF-β1 was added to HK-2 cells to construct the RIF model for 24 h at 37˚C; iv) in the OE-NKILA group, Lv-NKILA was used for transfection and cells were collected after 24 h at 37˚C Lv transfection; v) in the control + KD-NC group, HK-2 cells were induced by adding 10 ng/ml TGF-β1, transfected with KD-NC virus (LVCON313) at the same time and collected after 24 h stimulation; vi) in the control + KD-NKILA2 group, HK-2 cells were induced by adding 10 ng/ml TGF-β1, transfected with Lv-NKILA-shRNA and cells were collected after 24 h at 37˚C stimulation; vii) in the normal + DMSO group, 1 μl DMSO (cat. no. D8371; Beijing Solarbio Science & Technology Co., Ltd) was added to the normal group; viii) in the control + DMSO group, 10 ng/ml TGF-β1 and 1 μl DMSO were added and cells were collected after 24 h at 37˚C stimulation; ix) in the control + AG490 group, 10 ng/ml TGF-β1 was added, while 50 μM AG490 (cat. no. S1509; Beyotime Biotechnology) was added for intervention and cells were collected after a total of 24 h stimulation; and x) in the OE-NKILA + AG490 group, transfection was performed with OE Lv-NKILA and 50 μM AG490 was added at the same time and cells were collected after a total of 24 h at 37˚C stimulation. The GV513 vector was used to produce Lv-NKILA (76304). The GV493 viral vector was used to make Lv-NKILA-shRNA (108126) and Lv-NKILA-shRNA (108127), and standard negative control sequences (instead of an empty vector) were used for all control plasmids to ensure that no specific gene expression was produced during transfection. The gene specific part: Lv-NKILA-shRNA (108126) was GGAAGATATTGC TGCAGTTTG; the knockdown virus Lv-NKILA-shRNA (108127) was GGAGAAGTCACACGTTGATTG. The negative control lentivirus sequence was TTCTCCGAACGT GTCACGT. Lentiviral construction sequences as well as vector information are provided in Table I.

Cell Counting Kit-8 (CCK-8) assay. AG490 was dissolved in DMSO to a stock concentration of 100 mM. Logarithmically growing HK-2 cells were harvested, inoculated at $4x10^4$/ml and incubated for 24 h at 37˚C under 5% CO_2. AG490 concentration gradients (0, 10, 20, 30, 40, 50, 60, 70, 80, 90 and 100 μM) were set to induce cells for 24 h. CCK-8 (cat. no. BS350B; Biosharp Life Sciences) reagent was subsequently added away from light and incubated in an incubator at 37˚C and 5% CO_2 for 2 h. Optical density value (single wavelength, 450 nm) was used to calculate cell viability and screen out the most suitable AG490 intervention concentration. The experiment was repeated three times.

Western blot analysis. Cellular proteins were isolated using RIPA buffer (cat. no. AR0105; Wuhan Boster Biological Technology, Ltd.) and quantified using a BCA assay. A standard curve constructed from BSA absorbance values was used to determine sample concentrations, which were uniformly adjusted to 3 μg/μl. Samples were combined with 2X SDS-PAGE loading buffer and PBS, heated to 100˚C for 8 min to denature proteins, cooled and stored at -20˚C. Proteins (30 μg/lane) were separated on 8% SDS-PAGE gels (cat. no. AR0138; Wuhan Boster Biological Technology, Ltd.) and transferred to PVDF membranes (cat. no. 1212639; GVS S.p.A.). After blocking with 5% non-fat milk for 2 h at room temperature, membranes were incubated overnight at 4˚C with primary antibodies against fibronectin (FN; 1:1,000; cat. no. ab45688; Abcam), collagen I (Col1; 1:1,000; cat. no. ab138492; Abcam), vimentin (Vim; 1:1,000; cat. no. 10366-1-AP; Proteintech Group, Inc.), α-smooth muscle actin (α-SMA; 1:1,000; cat. no. 14395-1-AP; Proteintech Group, Inc.), JAK2 (1:1,000; cat. no. 17670-1-AP; Proteintech Group, Inc.), STAT3 (1:1,000; cat. no. 10253-2-AP; Proteintech Group, Inc.), phosphorylated (p)-JAK2 (1:500; cat. no. ab32101; Abcam), p-STAT3 (1:500; cat. no. ab76315; Abcam) and GAPDH (1:5,000; cat. no. 10494-1-AP; Proteintech Group, Inc.). Following TBS-1% Tween washes, membranes were incubated with HRP-conjugated goat anti-rabbit IgG (1:10,000; cat. no. BA1054; Wuhan Boster Biological Technology, Ltd) for 1 h at 25˚C. The blots were developed using an ECL reagent (cat. no. BL520A; Biosharp Life Sciences) and imaged using a Chemstudio system (Analytik Jena.). Band intensities were quantified in ImageJ (ImageJ Launcher1.4.3.67; National Institutes of Health) with GAPDH as the loading control. The experiments were repeated 3 times.

Immunofluorescence and imaging analysis. HK-2 cells were seeded on cell slides 14 mm in diameter at a density of $2x10^4$/well. HK-2 cells were rinsed in 1X PBS and subsequently fixed in 4% paraformaldehyde for 30 min at room temperature. After 0.5% Triton-100 permeabilization for 10 min at room temperature, 5% normal goat serum (Sigma-Aldrich; Merck KGaA) blocking for 30 min at room temperature and PBS washing was performed. Samples were incubated with epithelial (E)-cadherin diluted in 1X PBS (1:50; cat. no. ab231303; Abcam) primary antibody overnight at 4˚C. Subsequently,

Table I. Lentiviral construction sequences.

Name	Lv no.	Sequence	Base pairs
OE-NKILA	Lv-NKILA (76304)	Forward primer	AGGTCGACTCTAGAGGATCCAGACCCGGCACCCGCGC AACGGAGGAG
		Reverse primer	ACCGTAAGTTATGTGCTAGCTCCAGTTAAATTGAGATAT ACTTACAC
KD-NKILA1	Lv-NKILA-shRNA (108126)	Forward primer	CCGGGGAAGATATTGCTGCAGTTTGCTCGAGCAAACTG CAGCAATATCTTCCTTTTTG
		Reverse primer	AATTCAAAAAGGAAGATATTGCTGCAGTTTGCTCGAGC AAACTGCAGCAATATCTTCC
KD-NKILA2	Lv-NKILA-shRNA (108127)	Forward primer	CCGGGGAGAAGTCACACGTTGATTGCTCGAGCAATCA ACGTGTGACTTCTCCTTTTTG
		Reverse primer	AATTCAAAAAGGAGAAGTCACACGTTGATTGCTCGAG CAATCAACGTGTGACTTCTCC
KD-NC	LVCON313	Forward primer	CCGGTTCTCCGAACGTGTCACGTTTCAAGAGAACGTGA CACGTTCGGAGAATTTTTG
		Reverse primer	AATTCAAAAATTCTCCGAACGTGTCACGTTCTCTTGAA ACGTGACACGTTCGGAGAA
OE-NC	LVCON335	Forward primer	CCGGTTCTCCGAACGTGTCACGTTTCAAGAGAACGTGA CACGTTCGGAGAATTTTTG
		Reverse primer	AATTCAAAAATTCTCCGAACGTGTCACGTTCTCTTGAA ACGTGACACGTTCGGAGAA

The lentiviral vectors containing oe-NKILA and oe-NC were loaded into GV513 with the sequence of Ubi-MCS-CBh-gcGFP-IRES-puromycin. The lentiviral vectors containing kd-NKILA1, kd-NKILA1 and KD-NC were loaded into GV493 with the sequence of hU6-MCS-CBh-gcGFP-IRES-puromycin. Lv, lentivirus; OE, overexpression; NC, negative control; KD, knockdown; MCS, multiple cloning site; IRES, internal ribosome entry site.

1X PBS diluted CoraLite594-conjugate goat anti-rabbit IgG (1:200; cat. no. ab6721; Abcam) were incubated in the dark at 37˚C for 1 h. The cells were stained with DAPI in dark for 2 min at room temperature, then washed with 1X PBS. Stained cells were visualized using a fluorescence microscope and the exposure time was 4 sec (Leica Application Suite X3.7.5.24914; Leica Microsystems). The experiments were repeated three times.

RNA extraction and RT-qPCR. Total RNA was isolated from cells using the RNApure Tissue & Cell Kit (cat. no. CW0584S; Jiangsu CoWin Biotech Co., Ltd.) and reverse transcribed into cDNA with the corresponding synthesis kit (cat. no. CW2569M; Jiangsu CoWin Biotech Co., Ltd.) according to the manufacturer's protocol. RNA concentration and purity were assessed using a NanoDrop™ 2000 system (cat. no. 840-317500, Thermo Fisher Scientific, Inc.), with A260/A280 ratio of 1.8-2.2. All cDNA samples were standardized to a concentration of 1,000 ng/μl and prepared as 20 μl reaction systems for subsequent assays. qPCR was carried using a ProFlex™ PCR System (cat. no. 4484073, Thermo Fisher Scientific, Inc.) with UltraSYBR mixture (cat. no. CW2601H; Jiangsu CoWin Biotech Co., Ltd.). The thermocycling conditions were as follows: Pre-denaturation step was performed at 95˚C for 10 min; denaturation was carried out at 95˚C for 15 sec; annealing and extension were conducted simultaneously at 60˚C for 15 sec; and a total of 40 cycles were completed. Gene-specific primers employed in the presented study are listed in Table II. Target gene expression levels were normalized to GAPDH and relative quantification was determined using the $2^{-\Delta\Delta Cq}$ method (30). The experiments were repeated three times.

Statistical analysis. All data were analyzed and plotted using GraphPad Prism 10.3 software (Dotmatics). The normality of data distribution was assessed using the Shapiro-Wilk normality test, $P>0.05$ indicated that the data were normally distributed. Normally distributed data are presented as mean ± standard deviation. Comparisons between two independent groups of were analyzed using an unpaired, two-tailed Student's t-test. Comparisons among multiple groups were performed using one-way analysis of variance followed by Tukey's honestly significant difference test. $P<0.05$ was considered to indicate a statistically significant difference. All experiments were repeated at least three times.

Results

LncRNA NKILA is potentially associated with JAK2/STAT3-mediated RIF. After filtering out the known mRNA and transcript variant (<200 bp) the HK-2 cell samples included 21,924 transcripts going through quality control of raw data, alignment and assembly. The raw sequence datasets reported

Table II. Gene primers used for reverse transcription-quantitative PCR.

Gene	Sequence	Base pairs
Vimentin	Forward primer	CCTTCGTGAATACCAAGACCTGCTC
	Reverse primer	AATCCTGCTCTCCTCGCCTTCC
α-smooth muscle actin	Forward primer	CTTCGTTACTACTGCTGAGCGTGAG
	Reverse primer	CCATCAGGCAACTCGTAACTCTTCTC
Epithelial cadherin	Forward primer	GCCATCGCTTACACCATCCTCAG
	Reverse primer	CTCTCTCGGTCCAGCCCAGTG
Fibronectin	Forward primer	GGCGACAGGACGGACATCTTTG
	Reverse primer	GGCACAAGGCACCATTGGAATTTC
Collagen I	Forward primer	TGGCAAAGAAGGCGGCAAAGG
	Reverse primer	AGGAGCACCAGCAGGACCATC
Janus kinase-2	Forward primer	CCAAAGTGGGCAGAATTAGCAAACC
	Reverse primer	TCGTATGATGGCTCTGAAAGAAGGC
STAT3	Forward primer	CACCAAGCGAGGACTGAGCATC
	Reverse primer	AGCCAGACCCAGAAGGAGAAGC
GAPDH	Forward primer	GGAGCGAGATCCCTCCAAAAT
	Reverse primer	GGCTGTTGTCATACTTCTCATGG

Table III. Interval distribution statistics of gene expression values in samples.

Sample	0-0.1 FI (%)	0.1-0.3 FI (%)	0.3-3.57 FI (%)	3.57-15 FI (%)	15-60 FI (%)	>60 FI (%)
Control_1	38058 (56.37)	5941 (8.80)	17052 (25.25)	4795 (7.10)	1333 (1.97)	341 (0.51)
Control_2	38998 (57.76)	5779 (8.56)	16566 (24.53)	4572 (6.77)	1281 (1.90)	324 (0.48)
Control_3	37468 (55.49)	6291 (9.32)	17453 (25.85)	4717 (6.99)	1276 (1.89)	315 (0.47)
Normal_1	37621 (55.72)	5989 (8.87)	17491 (25.90)	4834 (7.16)	1282 (1.90)	303 (0.45)
Normal_2	36799 (54.50)	6086 (9.01)	17931 (26.56)	5044 (7.47)	1360 (2.01)	300 (0.44)
Normal_3	37120 (54.98)	5925 (8.78)	17776 (26.33)	5034 (7.46)	1349 (2.00)	316 (0.47)

FI, fragments per kilobase million interval.

in the present study have been submitted to the Genome Sequence Archive in the National Genomics Data Center (China National Center for Bioinformation/Beijing Institute of Genomics, Chinese Academy of Sciences; GSA-Human, HRA006966) publicly accessible at https://ngdc.cncb.ac.cn/gsa-human/browse/HRA006966. Inter-sample variability was observed in both the total number of detected genes and their expression magnitudes. To quantify this, genes were binned into discrete FPKM intervals and the count of genes falling within each interval was tallied for every library (Table III). According to the CPC (score ≤0.5), the prediction result of protein-coding potential was 12,347 (Fig. 1A). According to the CNCI (length, ≥200; exon numbers ≥1; score, ≤0), the prediction result of protein-coding potential was 10,617 (Fig. 1B). Using R, the FPKM value of the gene was taken as a parameter and INF_PVAL was set to $1x10^{-20}$. Clustering analysis revealed that 1,380 mRNAs (897 upregulated and 483 downregulated; Fig. 1C) and 1,147 lncRNAs (687 upregulated and 460 downregulated; Fig. 1D) were significantly differentially expressed between the two groups.

High-throughput sequencing identified 1,380 differentially expressed mRNAs, and GO enrichment analysis revealed significant associations with 1,127 biological functions. Based on significance rankings, the top 20 enriched functional categories were visualized, encompassing 'collagen-containing ECM', 'ECM organization', 'cell adhesion', 'extracellular region', 'extracellular space', 'plasma membrane', 'cell migration' and 'angiogenesis' (Fig. 1E).

Based on the analysis of differentially expressed lncRNAs, lncRNA NKILA was the most significantly cis-regulated target transcripts in TGF-β1-induced HK-2 cells compared with the normal groups and was increased in the RIF model (Table IV; Fig. 2A). The binding sites of NKILA promoter region were successfully predicted by JASPAR database. The lncRNA NKILA and STAT3 were found to have significant binding sites (Table V; Fig. 2B). Therefore, JAK2/STAT3 may be the putative regulatory pathway mediated by lncRNA NKILA.

LncRNA NKILA transfection assay. Compared with normal cultured HK-2 cells, the negative control lentivirus

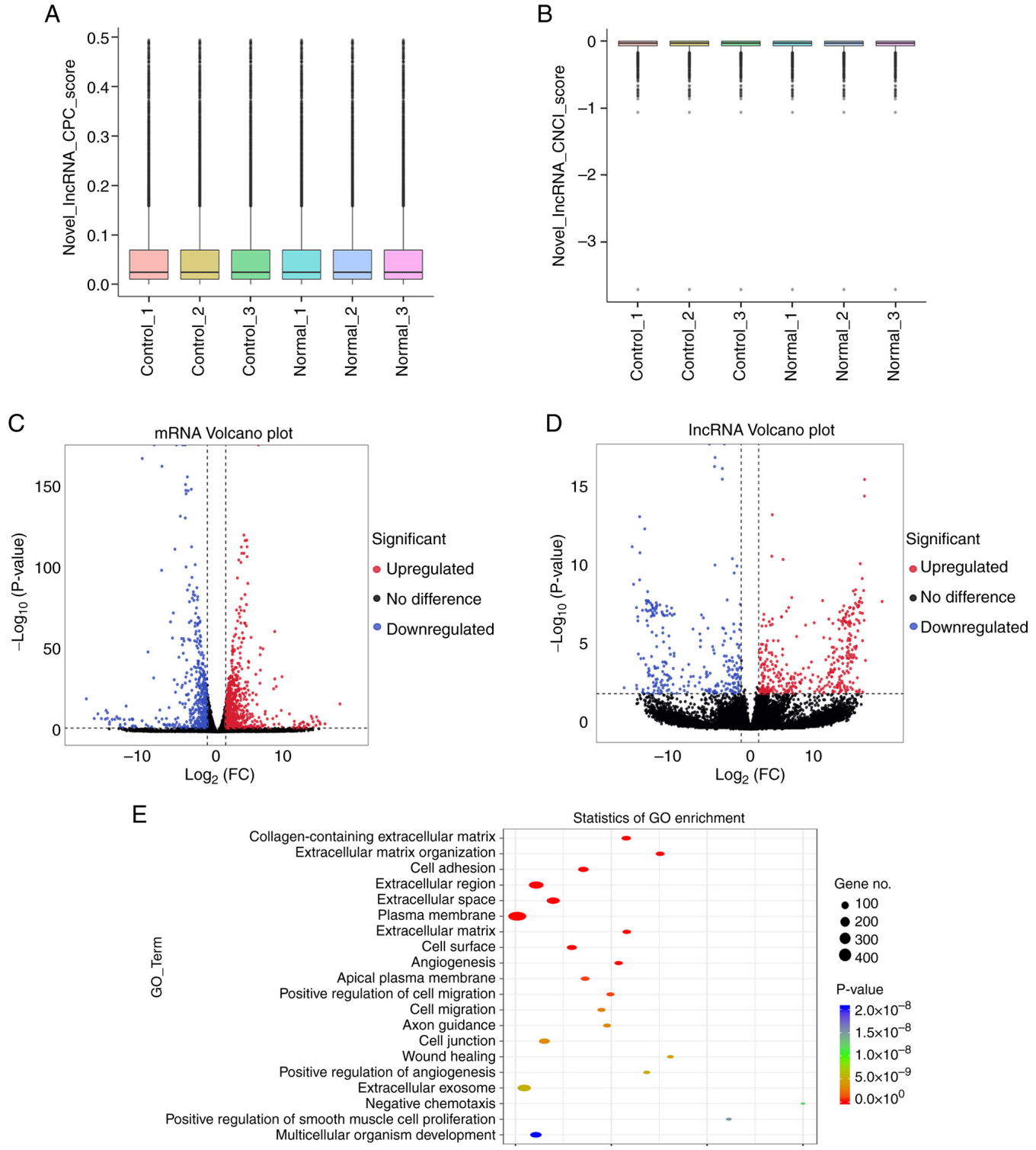

Figure 1. lncRNA high-throughput data sequencing. (A) lncRNA CPC score. CPC parameter was set as ≤0.5, and the predicted result was 12,347. (B) lncRNA CNCI score, CNCI parameters were set as length ≥200 bp, exon ≥1 and score ≤0 and the predicted result was 10,617. Volcano plots revealed (C) differentially expressed mRNAs and (D) differentially expressed lncRNAs between the normal groups (n=3) and the control group (n=3). Red represents upregulation, blue represents downregulation and black represents no significant difference. (E) Top 20 terms in GO enrichment analysis. lncRNA, long non-coding RNA; CPC, Coding Potential Calculator CNCI, Coding-Non-Coding Index; GO, Gene Ontology; FC, fold change.

(LVCON335) did not produce biological effects. Compared with normal HK-2 cells and LVCON335 transfected cells, the expression level of lncRNA NKILA was significantly increased after transfected with OE-NKILA lentivirus. Similarly, transfection of the lentiviral negative control (LVCON313) did not produce any biological effect in normal cell culture HK-2 cells, but the expression of lncRNA NKILA was significantly reduced in normal HK-2 cells transfected with two different fragments of lncRNA NKILA knockdown virus (Fig. 3).

Table IV. Top five significantly cis-regulated target transcripts in the control vs. normal groups.

ID	Length (bp)	Gene name	log_2 (FC)	P-value	Regulation
ENST00000614771	2625	NKILA	2.926772479	$1.15x10^{-34}$	Up
ENST00000667822	1630	AL050403	3.994934816	$2.33x10^{-18}$	Up
ENST00000599209	598	AC008687	4.053600164	$9.00x10^{-18}$	Up
ENST00000517664	3549	AC022893	-13.14250225	$6.21x10^{-17}$	Down
ENST00000666405	2930	VAC14-AS1	-13.12616293	$7.42x10^{-16}$	Down

FC, fold change.

Table V. Prediction results of binding sites.

Matrix ID	Name	Relative score (%)	Start	End	Predicted sequence
MA0144.2	MA0144.2.STAT3	88.33	1308	1318	TTGCAGAGAAG
MA0144.2	MA0144.2.STAT3	87.19	585	595	GAGCTGGGAAC
MA0144.2	MA0144.2.STAT3	87.00	1551	1561	TTGTCTGAAAG

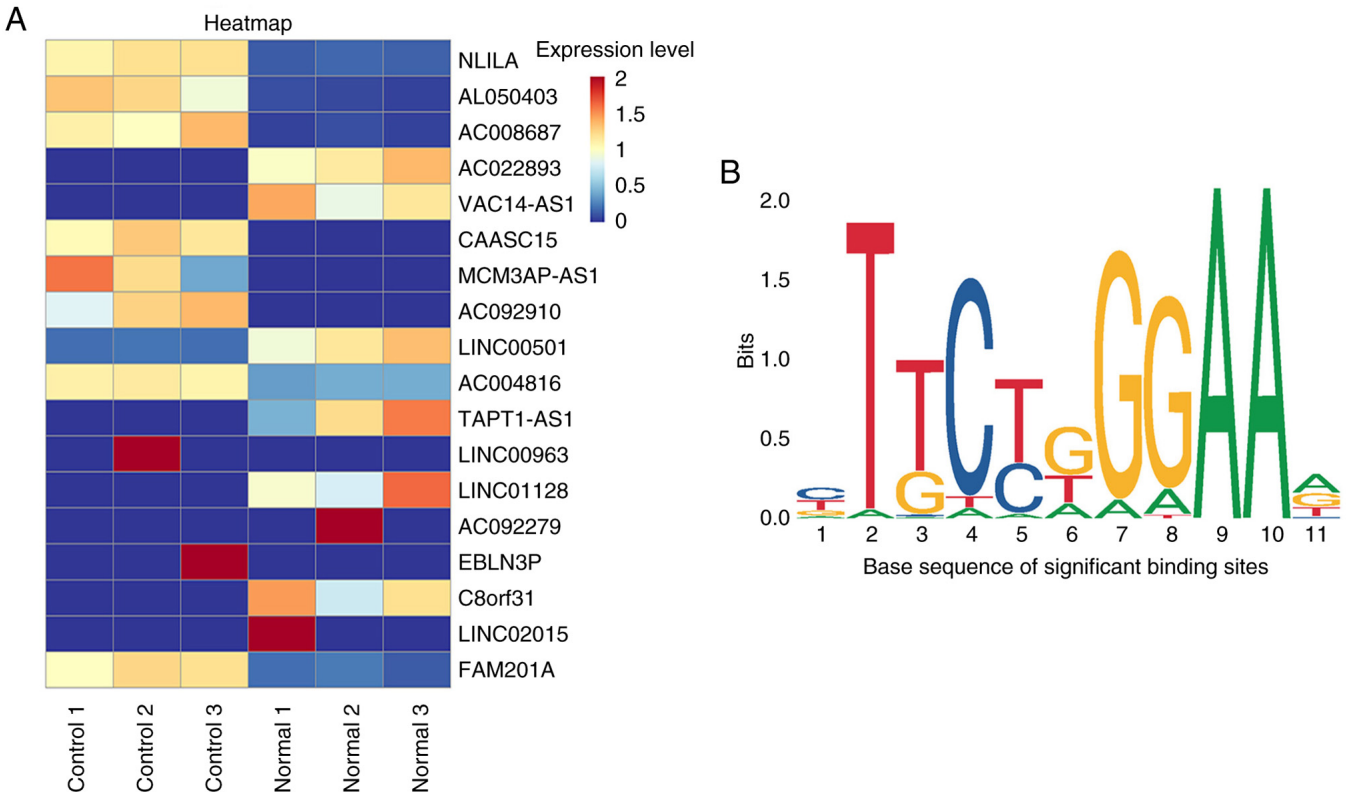

Figure 2. Heat map analysis of the top 20 cis-regulated lncRNAs in the lncRNA high-throughput sequencing and the binding and site results of the NKILA promoter region predicted by JASPAR database. (A) Heatmap demonstrating the top 20 cis-regulated lncRNAs in the control group compared with the normal group. 'Normal' indicates blank groups and 'control' indicates TGF-β1 (10 ng/ml) induced HK-2 cells. Y-axis shows cis-regulated lncRNA corresponding names. Color changes represent the expression level of the control group changes after normalization treatment compared with the blank group. The change from blue to red after normalization ranges from 0-2. (B) STAT3 binding site information predicted by the JASPAR database for the promoter region from 2000-99 bp upstream of NKILA. lncRNA, long non-coding RNA.

LncRNA NKILA OE facilitates EMT of HK-2 cells through the JAK2/STAT3 pathway. To assess the regulatory role of lncRNA NKILA in EMT through the JAK2/STAT3 pathway, HK-2 cells were transduced with either lncRNA OE-NKILA or an empty vector control (OE-NC). Compared with the OE-NC group, OE-NKILA significantly upregulated mesenchymal

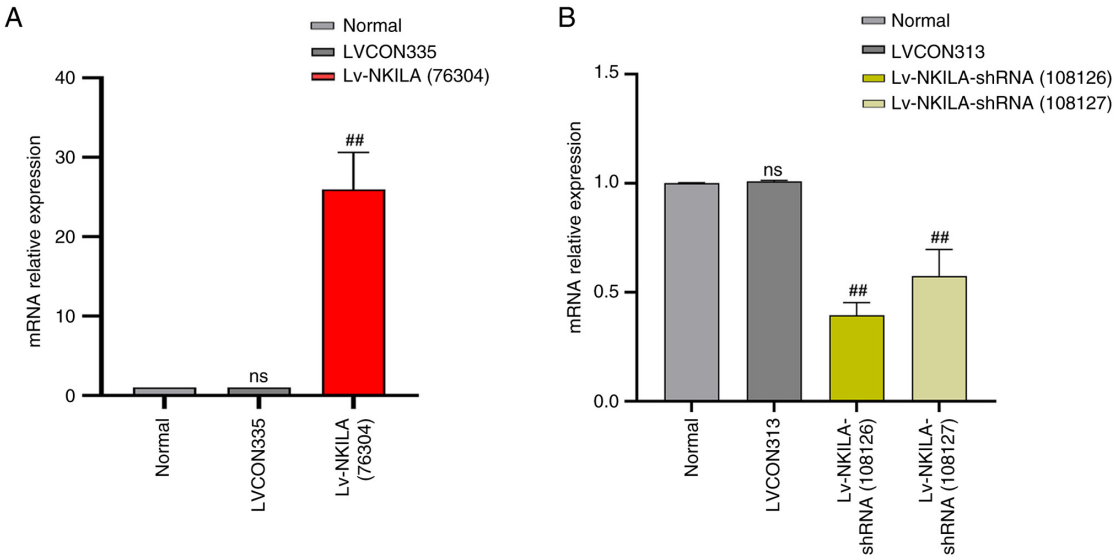

Figure 3. lncRNA NKILA overexpression lentivirus and negative control lentivirus transfection experiments. (A) Relative expression level of NKILA after transfection with Lv-NKILA detected by RT-qPCR (n=3). (B) Relative expression levels of NKILA after transfection with Lv-NKILA-shRNA and Lv-NKILA-shRNA (n=3) detected by RT-qPCR. LVCON313 indicates transfection of the knockdown negative control virus LVCON313. LVCON335 indicates transfection of the overexpressed negative control virus LVCON335. Lv-NKILA (76304) indicates transfection of overexpressing Lv-NKILA (76304) in normally cultured HK-2 cells (MOI=5). Lv-NKILA-shRNA (108126) indicates transfection of the knockdown virus Lv-NKILA-shRNA (108126) in normally cultured HK-2 cells (MOI=5). Lv-NKILA-shRNA (108127) indicates transfection of the knockdown virus Lv-NKILA-shRNA (108127) in normally cultured HK-2 cells (MOI=5). $^{##}$P<0.01 compared with the normal group. RT-qPCR, reverse transcription quantitative PCR; MOI, multiplicity of infection; shRNA, short hairpin; Lv, lentivirus.

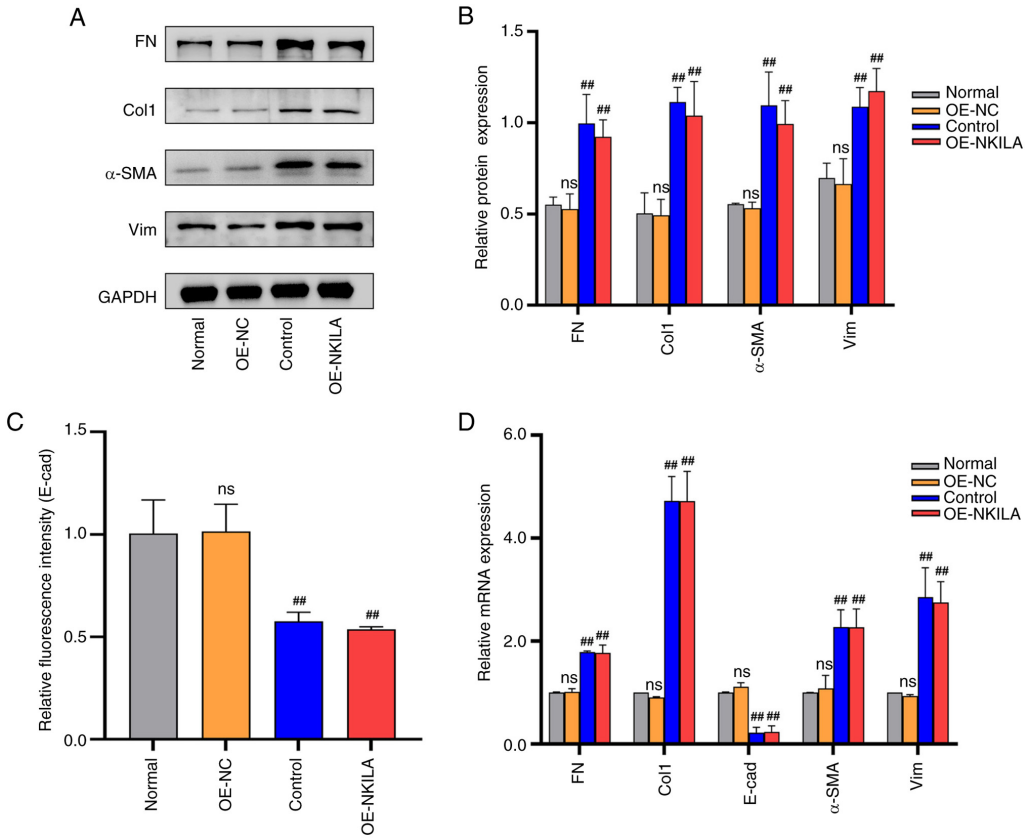

Figure 4.Partial EMT phenotype proteins in HK-2 cells transfected with lncRNA NKILA overexpression virus (A) Representative western blotting images and (B) quantification of EMT phenotypic indicators. (C) Statistical analysis results of E-cad fluorescence intensity (n=3). (D) RT-qPCR statistical results of EMT phenotype indicators (n=3). 'Normal' indicates after starvation treatment, HK-2 cells were replaced with fresh complete medium and continued to be cultured for 24 h. Control, following starvation treatment, 10 ng/ml TGF-β1 cytokine diluent was added to induce HK-2 cells to construct the renal interstitial fibrosis model for 24 h. 'OE-NKILA' indicates after starvation, overexpressed Lv-NKILA (76304) was used for transfection and cells were collected after 24 h of lentivirus transfection. Compared with OE-NC $^{##}$P<0.01. E-cad; epithelial-cadherin; RT-qPCR, reverse transcription quantitative PCR; EMT, epithelial-mesenchymal transition; NC, negative control; Lv, lentivirus; OE, overexpression; FN, fibronectin; Col1, collagen I; α-SMA, α-smooth muscle actin; Vim; vimentin; ns, not significant.

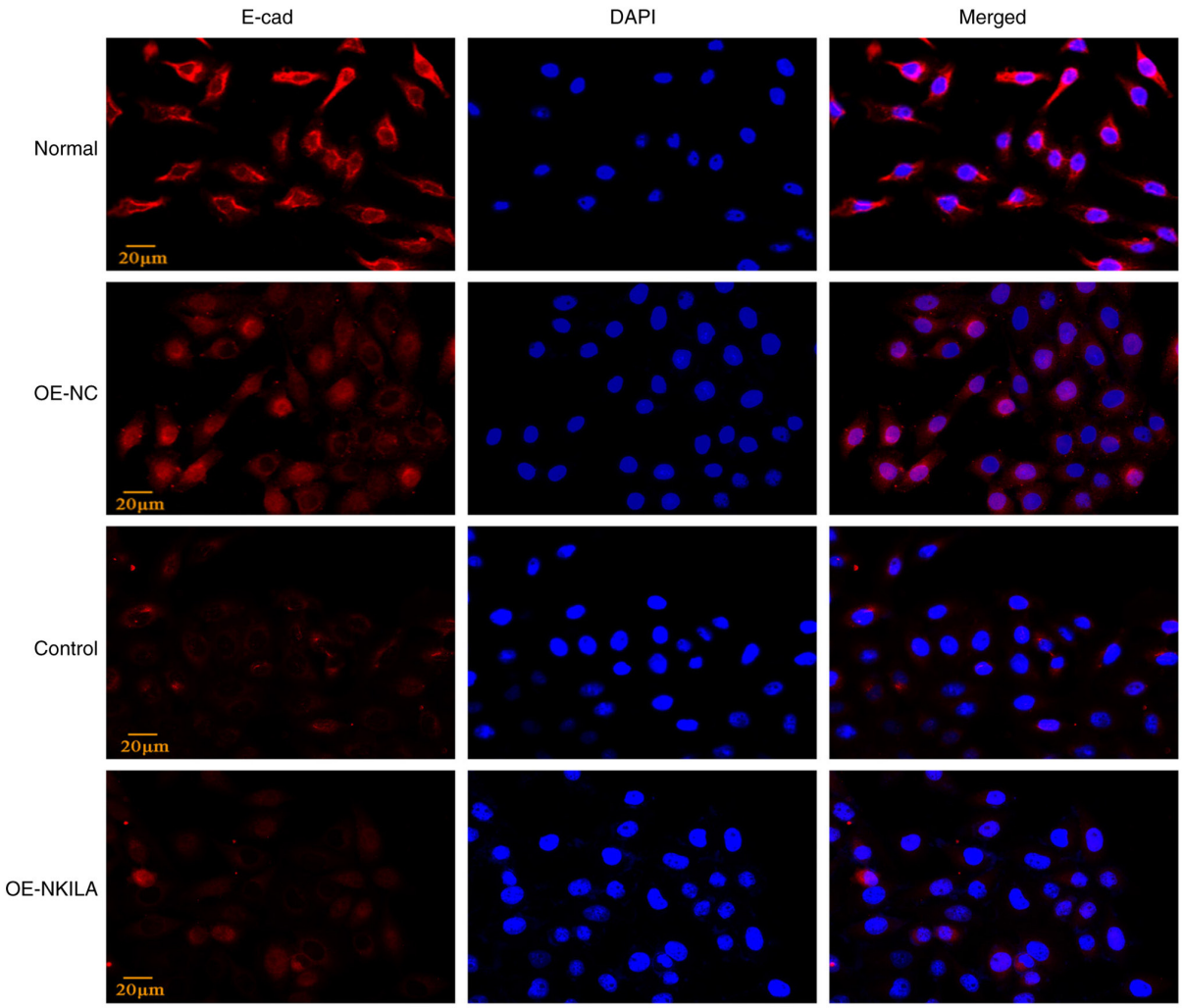

Figure 5. Immunofluorescence of E-CAD protein following lncRNA NKILA OE transfection experiments. Expression of E-cad observed by immunofluorescence (magnification, x400; scale bar, 20 μm; n=3) compared with the normal group. OE, overexpression; E-cad, epithelial-cadherin; NC, negative control.

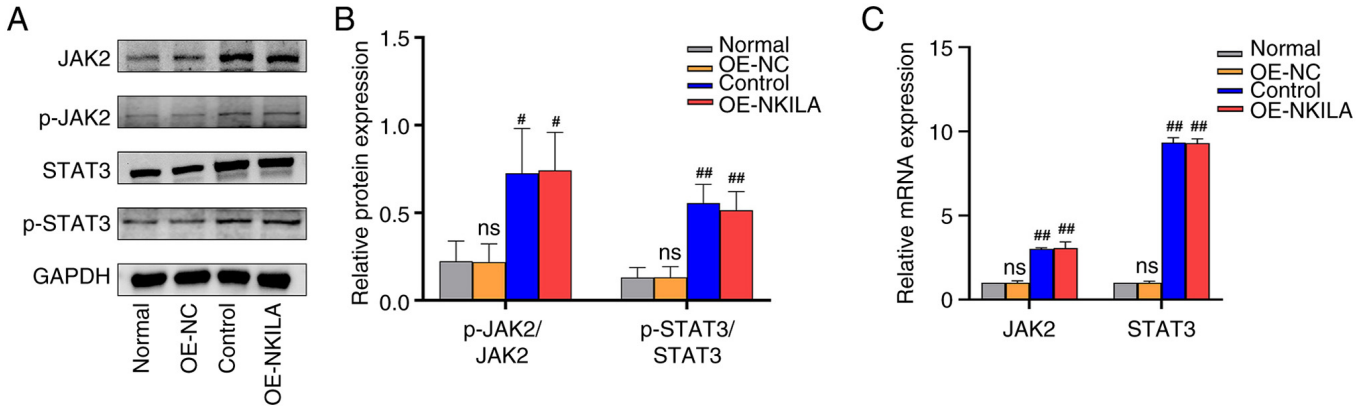

Figure 6.JKA2/STAT3 pathway protein detection in HK-2 cells transfected with LncRNA NKILA overexpression virus (A) Representative western blotting bands and (B) semi-quantification of results of protein expression of phosphorylated JAK2 and STAT3 (n=3). (C) RT-qPCR statistical results (n=3). $^{\#\#}$P<0.01 and $^{\#}$P<0.05 compared with the normal group. ns, not significant; p-, phosphorylated; OE, overexpression; NC, negative control; JAK, Janus kinase; RT-qPCR, reverse transcription quantitative PCR.

markers (FN, Col1, α-SMA and Vim) and downregulated the epithelial marker E-cadherin, as determined by RT-qPCR and western blotting (Fig. 4). Immunofluorescence staining further demonstrated a reduction in E-cadherin expression in OE-NKILA-treated cells compared with the controls, indicating enhanced EMT progression (Figs. 4 and 5). Compared with the normal control group and the OE-NC group, both the phosphorylation ratio of JAK2 (p-JAK2/JAK2) and that

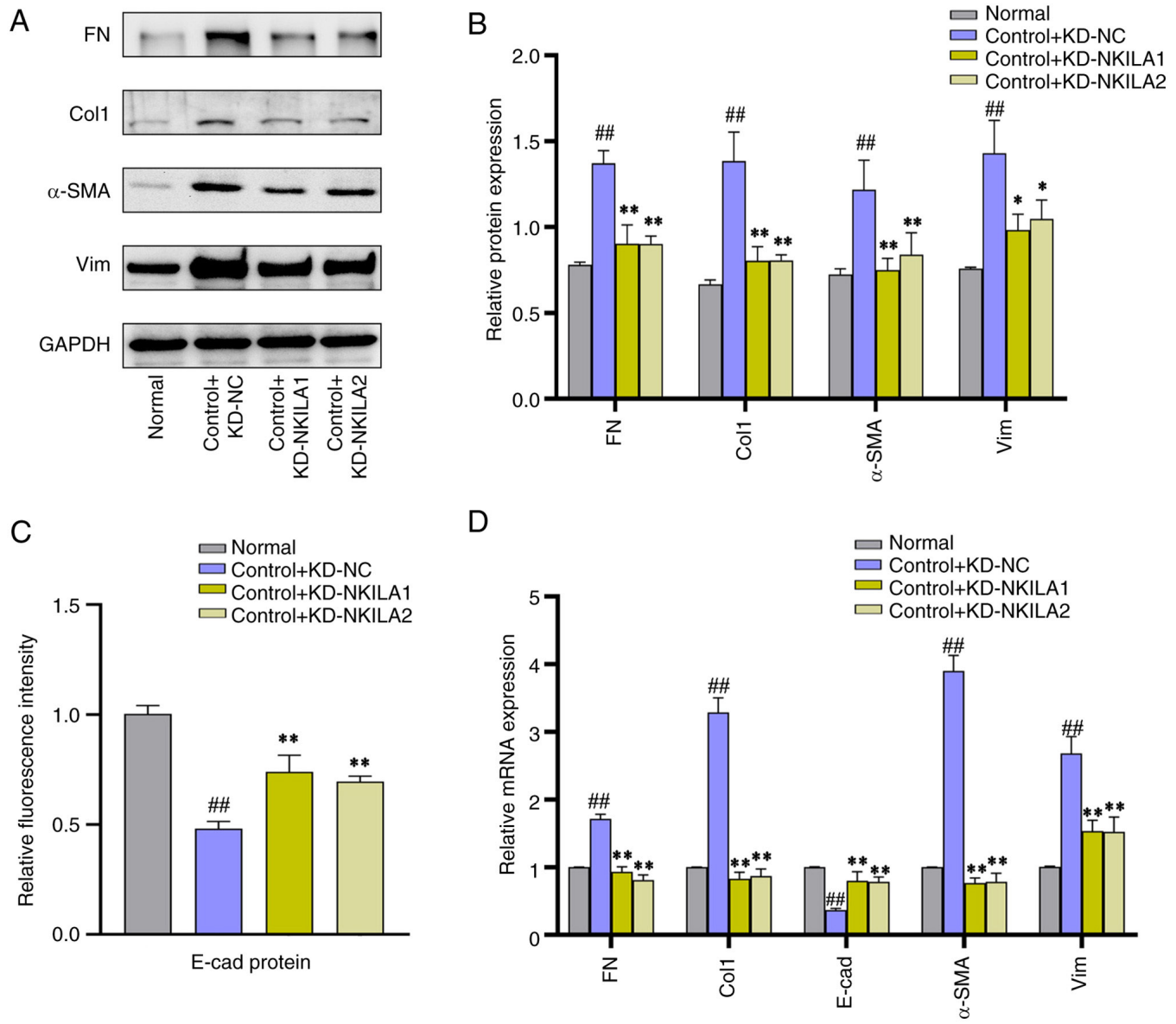

Figure 7. Partial EMT phenotype proteins in HK-2 cells transfected with lncRNA NKILA knockdown lentivirus (A) Representative western blotting bands and (B) semi-quantification results of EMT phenotypic indicators. (C) E-cad fluorescence intensity and (D) EMT phenotypic index RT-qPCR (n=3). 'Normal' indicates starvation treatment. Compared with normal group $^{\#\#}$P<0.01. Compared with control + KD-NC group, **P<0.01 and *P<0.05. EMT, epithelial-mesenchymal transition; E-cad, epithelial-cadherin; RT-qPCR, reverse transcription quantitative PCR; KD, knockdown; Lv, lentivirus; shRNA, short hairpin RNA; NC, negative control; FN, fibronectin; Col1, collagen I; α-SMA, α-smooth muscle actin; Vim; vimentin.

of STAT3 (p-STAT3/STAT3) were significantly elevated in the control and the OE-NKILA group. Consistent with these protein-level findings, qPCR analysis revealed a corresponding upregulation in the expression of relevant downstream targets, these results suggest that lncRNA NKILA promotes EMT through activation of the JAK2/STAT3 pathway (Fig. 6).

KD of lncRNA NKILA attenuates EMT in HK-2 cells and inhibits the activation of JAK2/STA3 pathway. In addition, two different lncRNA NKILA-KD lentiviruses (control + KD-NKILA1 and control + KD-NKILA2) and their NC were transfected into HK-2 cells to establish the model of EMT induced by TGF-β1. Compared with control + KD-NC group, NKILA KD significantly suppressed mesenchymal markers, FN, Col1, α-SMA and Vim, at both transcript and protein levels. Of note, E-cadherin expression was consistently elevated upon NKILA depletion, as demonstrated through RT-qPCR and immunofluorescence analyses (Figs. 7 and 8). Collectively, Compared with the control + KD-NC group, The ratio of P-JAK2 to JAK2 protein and P-STAT3 to STAT3 protein in NKILA KD group (control + KD-NKILA1 and control + KD-NKILA2) were significantly decreased, these findings suggest that lncRNA NKILA is key in preventing EMT under TGF-β1 conditions and inhibiting the JAK2/STAT3 pathway (Fig. 9).

lncRNA NKILA interferes with the fibrotic process of HK-2 cells by regulating the JAK2/STAT3 pathway. Through the OE and KD of lncRNA NKILA experiments, lncRNA NKILA was demonstrated to initiate the fibrosis of HK-2 cells and NKILA may serve a fibrogenic role by regulating the JAK2/STAT3 signaling pathway. In order to validate these findings, AG490, a specific inhibitor of the JKA2/STAT3 signaling pathway, was

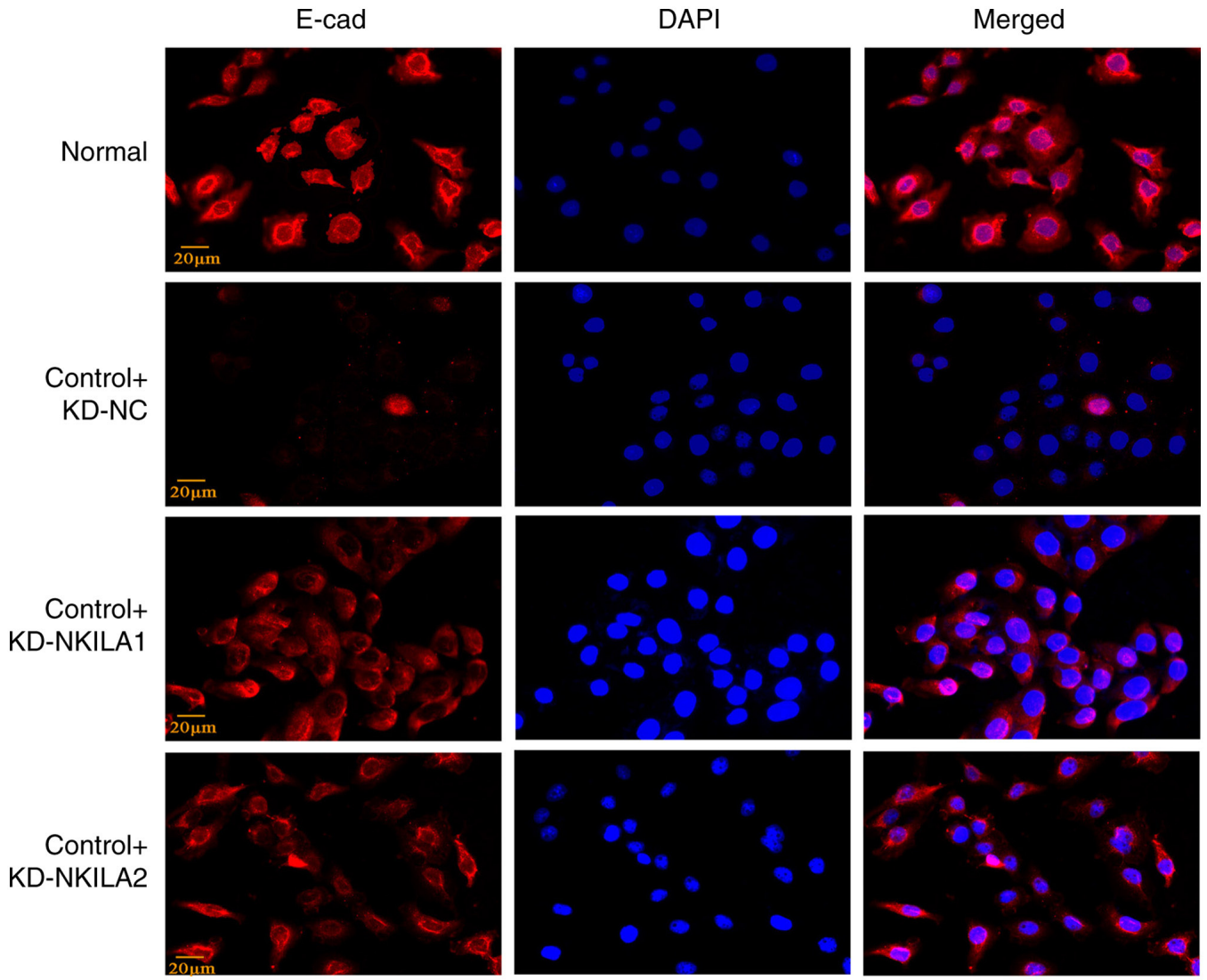

Figure 8. Immunofluorescence detection of E-CAD protein following KD of lncRNA NKILA experiment Expression of E-cad observed by immunofluorescence (magnification, x400; scale bar, 20 μm; n=3) compared with the normal group. E-cad, epithelial cadherin; KD, knockdown; NC, negative control.

introduced for further experimental verification. The optimal administration concentration of AG490 was screened using the CCK-8 method. Findings revealed that the IC_{50} value was 45.43 μM. The present study examined the viability of HK-2 cells in a concentration gradient ranging from 10 to 100 μM and found no significant difference in cell viability in a molar concentration gradient ranging from 50 to 80 μM. However, since AG490 requires the use of DMSO for dissolution, to avoid excessive damage to HK-2 cells and affect the experimental results, the intervention dose of AG490 used in the present experiment was 50 μM (Fig. 10). Subsequently, AG490 was used to treat the TGF-β1-induced HK-2 cell RIF model and NKILA-induced HK-2 cell EMT model. Compared with the normal control group, no significant difference was observed in the phosphorylation ratios of JAK2 and STAT3 in the normal + DMSO group. The phosphorylation ratios of JAK2 and STAT3 in the control + DMSO group were comparable to those in the oe-NKILA group. In contrast, both ratios were significantly elevated in the oe-NKILA group relative to the control + DMSO group. Treatment with AG490 markedly suppressed JAK2 and STAT3 phosphorylation in both the control and oe-NKILA backgrounds: specifically, the p-JAK2/JAK2 and p-STAT3/STAT3 ratios were significantly reduced in the control + AG490 group compared with the control + DMSO group, and similarly decreased in the oe-NKILA + AG490 group relative to the oe-NKILA group (Fig. 11). DMSO had no effect on EMT markers vs. normal controls. The control+ DMSO and oe-NKILA groups both showed significant EMT induction (upregulated FN, Col1, Vim, α-SMA; downregulated E-CAD). AG490 treatment markedly reversed this phenotype, suppressing mesenchymal markers and restoring E-CAD in both control and oe-NKILA groups (Figs. 12 and 13). Collectively, these data indicate that NKILA modulates the JAK2/STAT3 axis and thereby attenuates the fibrogenic response in HK-2 cells.

Discussion

RIF, characterized by abnormal accumulation of collagen and other ECM proteins in the tubulointerstitial compartment, is a frequent histological finding in diverse renal pathologies (31). In CKD progression, EMT drives ECM remodeling and

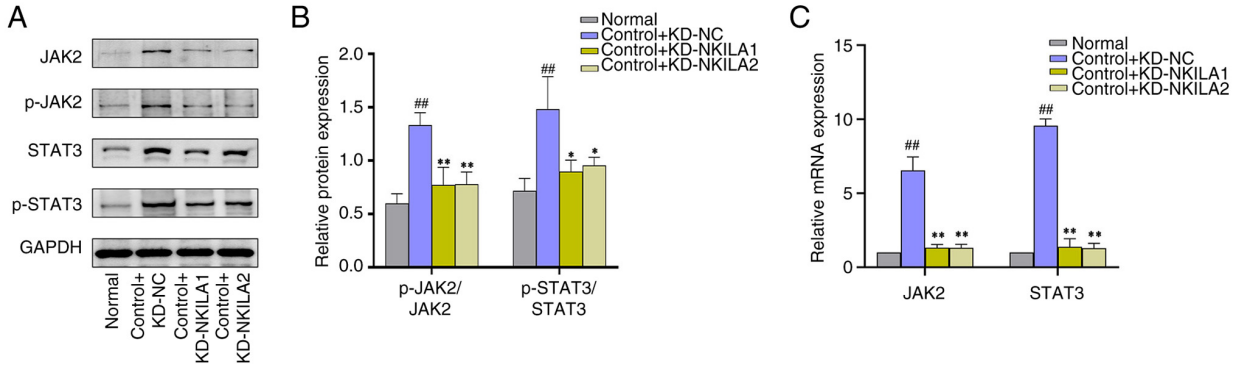

Figure 9. JAK2/STAT3 signaling pathway-associated proteins in HK-2 cells transfected with LncRNA NKILA knockdown lentivirus (A) Representative western blotting bands and (B) semi-quantification of JAK2/STAT3 pathway protein expression (n=3). (C) Statistical analysis results of reverse transcription-quantitative PCR for channel indicators. ##P<0.01 compared with the normal group (n=3), **P<0.01 and *P<0.05 compared with the control + KD-NC group. JAK, Janus kinase; KD, knockdown; NC, negative control; p-, phosphorylated.

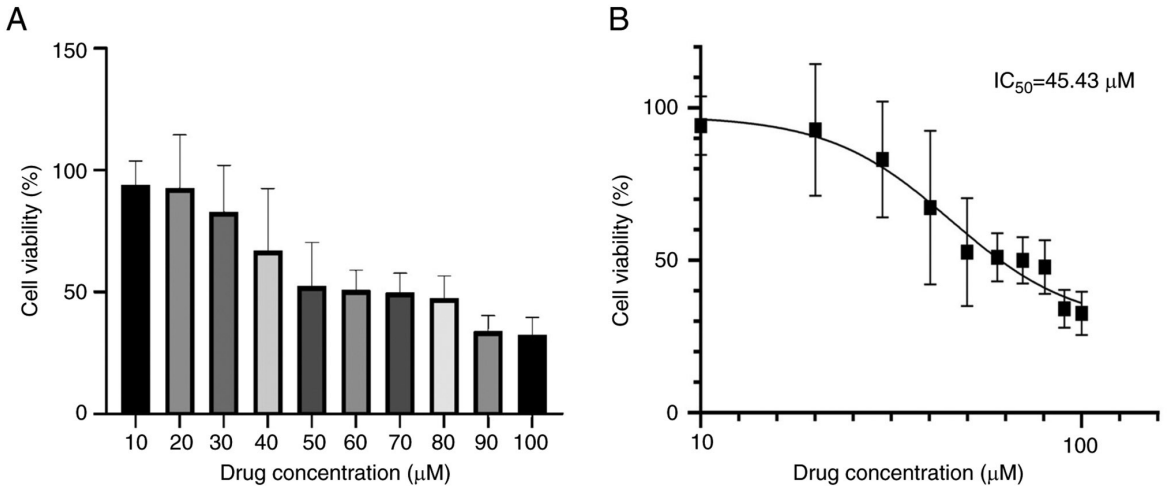

Figure 10. CCK8 test results (A) Cell survival ratio. (B) IC_{50} value was 45.43 μM. The intervention dose of AG490 used in the present experiment was 50 μM.

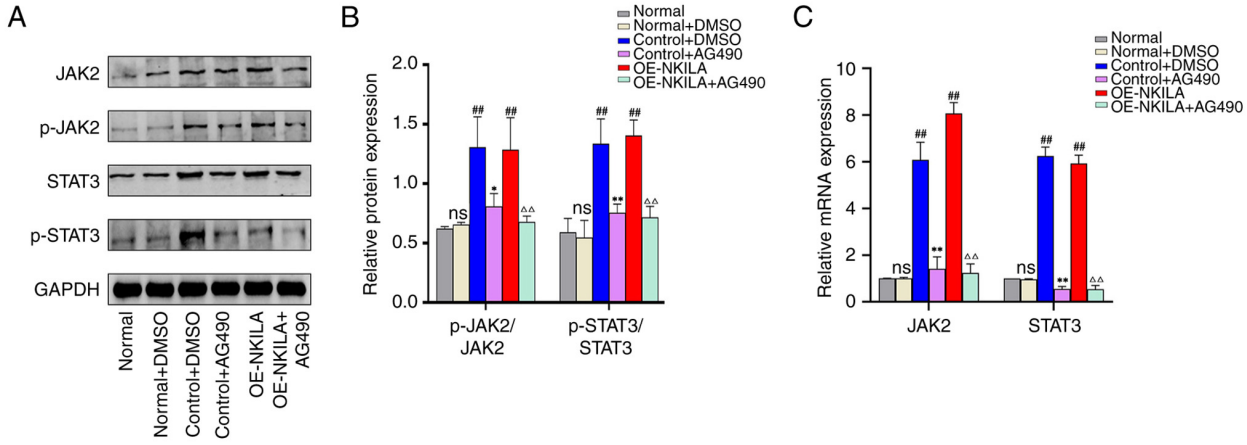

Figure 11. JAK2/STAT3 pathway protein detection in the recovery experiment of HK-2 cells treated with AG490. (A) Representative western blotting bands and (B) semi-quantification of JAK2/STAT3 pathway protein expression (n=3). (C) Reverse transcription-quantitative PCR for channel indicators (n=3). ##P<0.01 compared with the normal group, **P<0.01 and *P<0.05 compared with control + DMSO group and △△P<0.01 compared with OE-NKILA group. OE, overexpression; p-, phosphorylated; JAK, Janus kinase; ns, not significant.

promotes RIF development. Notably, evidence has supported the pathogenic role of EMT in renal repair processes. During initial EMT stages, injured epithelial cells trigger profibrotic signaling, leading to immune cell recruitment and subsequent activation. These infiltrating immune cells exacerbate fibrogenesis through sustained cytokine release (32).

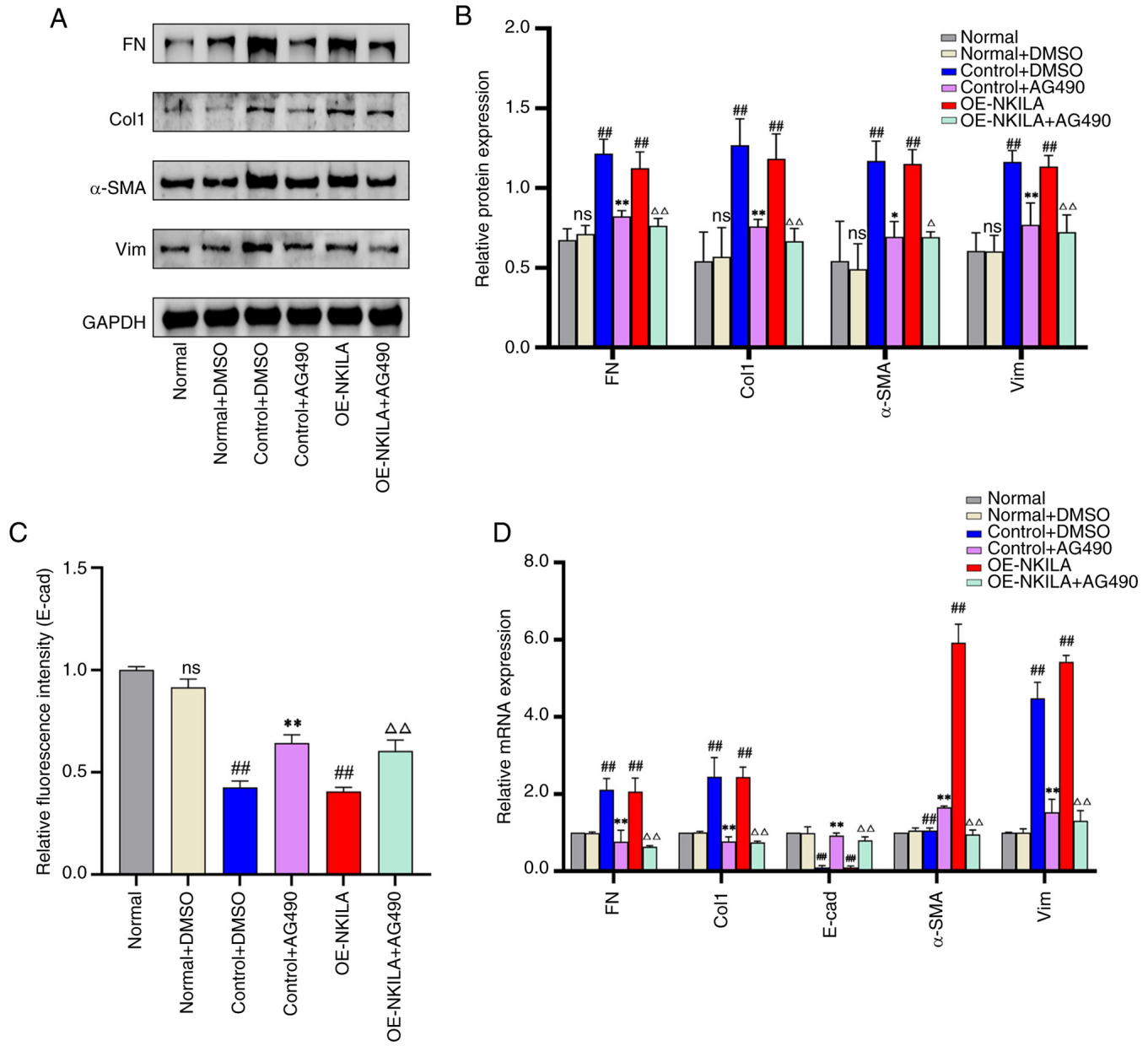

Figure 12. Detection of EMT-related phenotypic proteins in the AG490 intervention HK-2 cell recovery experiment (A) Representative western blotting bands and (B) semi-quantification of EMT phenotypic protein changes (n=3). (C) Statistical analysis results of E-cad fluorescence intensity (n=3) and (D) EMT phenotypic index through reverse transcription quantitative PCR (n=3). 'Normal' indicates starvation treatment, HK-2 cells were replaced with fresh complete medium and continued to be cultured for 24 h. $^{\#\#}$P<0.01 compared with the normal group, **P<0.01 and *P<0.05 compared with the control + DMSO group and $^{\triangle\triangle}$P<0.01 and $^{\triangle}$P<0.05 compared with the OE-NKILA group. EMT, epithelial-mesenchymal transition; E-cad, epithelial cadherin; OE, overexpression; Lv, lentivirus; FN, fibronectin; Col1, collagen I; α-SMA, α-smooth muscle actin; Vim; vimentin.

EMT is orchestrated by complex molecular networks involving multiple regulatory tiers. Key mechanisms encompass transcriptional activation, altered expression of specific cell-surface proteins, cytoskeletal remodeling and production of ECM-degrading enzymes. With the growing improvement in transcriptome sequencing technology, large numbers of lncRNAs have been reported to represent attractive intervention targets for cardiovascular and cerebrovascular, nervous system, tumor and EMT processes in previous studies (33-37). Understanding the functions and spatial structures of lncRNAs could therefore help to develop potential novel therapies.

lncRNA NKILA was identified and named as a NF-κB interacting lncRNA in breast cancer, with its main function being to bind to the NF-κB/IκB complex, inhibiting the NF-κB pathway by masking the phosphorylation site of IκB and stabilizing the complex (38-40). However, the interactions between fragments of NKILA and the NF-κB domain are weak and non-specific. At present, the studies on NKILA function mainly focus on the role of NKILA-NF-κB-IκBα in diseases such as cardiovascular and cerebrovascular disease, lung adenocarcinoma, liver cancer, esophageal squamous cell carcinoma and osteoarthritis from the perspective of protecting the NF-κB-IκBα complex from abnormal activation of the NF-κB signaling pathway (41-43). However, simultaneously, NKILA can be used as an independent risk factor for colorectal cancer, coronary heart disease, lung adenocarcinoma, Parkinson's

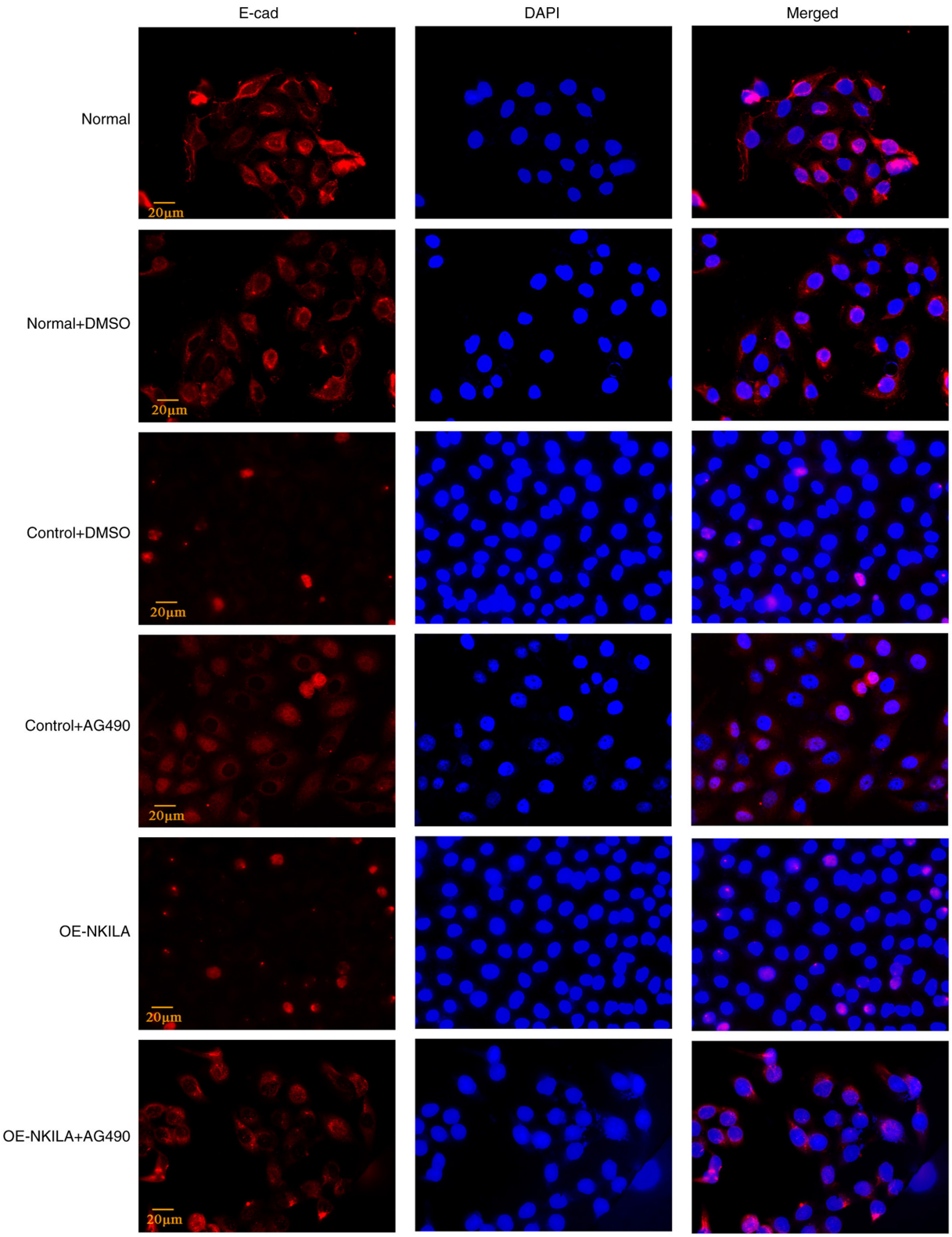

Figure 13. Immunofluorescence detection of E-CAD protein in the recovery experiment of HK-2 cells treated with AG490. E-cad immunofluorescence staining (magnification, x400; scale bar, 20 μm; n=3) compared with the normal group. E-cad, epithelial cadherin; OE, overexpression.

disease and type 2 diabetes (44-46). Due to a limited understanding of lncRNA NKILA, there is no unified standard to assess the change of lncRNA NKILA expression in different diseases. However, lncRNA NKILA has marked research potential, which may lead to an improved understanding of lncRNAs in diseases.

In the present study, EMT markers were assessed in HK-2 cells following stimulation with TGF-β1 or lncRNA NKILA. The data revealed that lncRNA NKILA OE elevated FN, Col1, α-SMA and Vim, while repressing E-cadherin, mirroring a pro-fibrotic EMT signature. Based on the biological functions of lncRNA NKILA, such as its involvement in

immune regulation and inflammatory response (47,48), the present results suggest that NKILA may activate inflammation-related signaling pathways in the process of fibrosis.

Following previous results of high-throughput sequencing analysis, the promoter region of lncRNA NKILA was demonstrated to have a possible binding site with STAT3. The JAK2/STAT3 pathway is dominant among various subtypes of JAK/STAT (49,50) and is a key signaling pathway involved in inflammation with phosphorylation as the main mode of action. The activation of this signaling pathway is implicated in driving fibrotic processes across multiple organs, including the lung, liver and kidneys. The role is mediated through its involvement in both inflammation and the induction of EMT (51-54). JAK2/STAT3 can be both an initiating factor and downstream in the process of renal fibrosis, which simultaneously respond to numerous cytokine signals to activate myofibroblasts and induce EMT (55).

The present study also demonstrated that the JAK2/STAT3 signaling pathway was activated in two different models of cell fibrosis (TGF-β1-induced and lncRNA NKILA-induced HK-2 cells), accompanied by the expression changes in EMT markers. In the rescue experiment with AG490, suppressing the expression of JAK2/STAT3 pathway notably reduced EMT changes in RIF cell models. On the one hand, the results demonstrated a potential key role of the JAK2/STAT3 signaling pathway in the progression of renal fibrosis. On the other hand, the results support the association between NKILA and the JAK2/STAT3 signaling pathway. Therefore, this suggests lncRNA NKILA has the potential to act as an independent stimulator of fibrosis in HK-2 cells through selective activation of the JAK2/STAT3 signaling pathway.

Although the present HK-2 cell model reveals the involvement of lncRNA NKILA in EMT-like changes and its interaction with the JAK2/STAT3 pathway during renal tubular EMT *in vitro*, the absence of *in vivo* validation limits its ability to fully represent the overall process of renal fibrosis. In future, the fibrogenic role of lncRNA NKILA may be further explored using *in vivo* experiments to evaluate its potential as an independent fibrogenic factor.

Acknowledgements

Not applicable.

Funding

The present study was funded by the National Famous Traditional Chinese Medicine Expert Inheritance Studio (grant no. 978022), Tianjin Health Research Project (grant no. TJWJ2024QN071) and the Scientific Research Project of the Administration of Traditional Chinese Medicine of Hebei Province (grant no. T2025046).

Availability of data and materials

The data generated in the present study may be found in the Genome Sequence Archive under BioProject number PRJCA024511, dataset number: HRA006966; DAC number: HDAC003863,or at the following https://ngdc.cncb.ac.cn/gsa-human/browse/HRA006966.

Authors' contributions

YH and YW designed the present study. YH, SY, JZ and HL performed the experiments and collected the data. YH and SY wrote the manuscript. YH,JZ and XZ were responsible for the data analysis of western blot detection. YH and JZ were responsible for CCK-8 data analysis and processing. YH and SY were responsible for q-PCR data analysis, immunofluorescence data analysis and processing, and high-throughput sequencing data visualization processing. YH and SY were responsible for the production and proofing of the pictures in the article. All authors read and approved the final version of the manuscript. YH and SY confirm the authenticity of all the raw data.

Ethics approval and consent to participate

Not applicable.

Patient consent for publication

Not applicable.

Competing interests

The authors declare that they have no competing interests.

References

1. Humphreys BD: Mechanisms of renal fibrosis. Annu Rev Physiol 80: 309-326, 2018.
2. Liu Y, Bi X, Xiong J, Han W, Xiao T, Xu X, Yang K, Liu C, Jiang W, He T, *et al*: MicroRNA-34a promotes renal fibrosis by downregulation of klotho in tubular epithelial cells. Mol Ther 27: 1051-1065, 2019.
3. Bülow RD and Boor P: Extracellular matrix in kidney fibrosis: More than just a scaffold. J Histochem Cytochem 67: 643-661, 2019.
4. Salminen A: Increased immunosuppression impairs tissue homeostasis with aging and age-related diseases. J Mol Med (Berl) 99: 1-20, 2021.
5. Lv JC and Zhang LX: Prevalence and disease burden of chronic kidney disease. Adv Exp Med Biol 1165: 3-15, 2019.
6. Mack M: Inflammation and fibrosis. Matrix Biol 68-69: 106-121, 2018.
7. GBD Chronic Kidney Disease Collaboration: Global, regional, and national burden of chronic kidney disease, 1990-2017: A systematic analysis for the Global Burden of Disease Study 2017. Lancet 395: 709-733, 2020.
8. Ali T and Grote P: Beyond the RNA-dependent function of LncRNA genes. Elife 9: e60583, 2020.
9. Bridges MC, Daulagala AC and Kourtidis A: LNCcation: LncRNA localization and function. J Cell Biol 220: e202009045, 2021.
10. Nojima T and Proudfoot NJ: Mechanisms of lncRNA biogenesis as revealed by nascent transcriptomics. Nat Rev Mol Cell Biol 23: 389-406, 2022.
11. Yang Z, Jiang S, Shang J, Jiang Y, Dai Y, Xu B, Yu Y, Liang Z and Yang Y: LncRNA: Shedding light on mechanisms and opportunities in fibrosis and aging. Ageing Res Rev 52: 17-31, 2019.
12. Xu J, Bai J, Zhang X, Lv Y, Gong Y, Liu L, Zhao H, Yu F, Ping Y, Zhang G, *et al*: A comprehensive overview of lncRNA annotation resources. Brief Bioinform 18: 236-249, 2017.
13. Fan XN, Zhang SW, Zhang SY and Ni JJ: lncRNA_Mdeep: An Alignment-free predictor for distinguishing long Non-coding RNAs from Protein-coding transcripts by multimodal deep learning. Int J Mol Sci 21: 5222, 2020.
14. Alaaeldin R, Ali FEM, Bekhit AA, Zhao QL and Fathy M: Inhibition of NF-kB/IL-6/JAK2/STAT3 pathway and epithelial-mesenchymal transition in breast cancer cells by azilsartan. Molecules 27: 7825, 2022.

15. Bird L: lncRNA NKILA: A killer regulator. Nat Rev Immunol 18: 666-667, 2018.
16. Dashti S, Ghafouri-Fard S, Esfandi F, Oskooei VK, Arsang-Jang S and Taheri M: Expression analysis of NF-κB interacting long noncoding RNAs in breast cancer. Exp Mol Pathol 112: 104359, 2020.
17. Soltanmoradi S, Tavakolpour V, Moghadasi AN and Kouhkan F: Expression analysis of NF-κB-associated long noncoding RNAs in peripheral blood mononuclear cells from relapsing-remitting multiple sclerosis patients. J Neuroimmunol 356: 577602, 2021.
18. Ghafouri-Fard S, Gholipour M, Abak A, Mazdeh M, Taheri M and Sayad A: Expression analysis of NF-κB-Related lncRNAs in Parkinson's disease. Front Immunol 12: 755246, 2021.
19. Tian S, Yu Y, Huang H, Xu A, Xu H and Zhou Y: Expression level and clinical significance of NKILA in human cancers: A systematic review and Meta-analysis. Biomed Res Int 2020: 4540312, 2020.
20. Li Y, Wang W, Chen K, Ma S and Wang J: Influence of LncRNA NKILA on bloodstream infection of hypervirulent klebsiella pneumoniae and its ability to induce delayed neutrophil apoptosis. Evid Based Complement Alternat Med 2021: 6101078, 2021.
21. Herman AB, Tsitsipatis D and Gorospe M: Integrated lncRNA function upon genomic and epigenomic regulation. Mol Cell 82: 2252-2266, 2022.
22. Martin M: Cutadapt removes adapter sequences from high-throughput sequencing reads. EMBnet J Bioinfo Action 17: 10-12, 2011.
23. Langmead B and Salzberg SL: Fast gapped-read alignment with Bowtie 2. Nat Methods 9: 357-359, 2012.
24. Kim D, Langmead B and Salzberg SL: HISAT: A fast spliced aligner with low memory requirements. Nat Methods 12: 357-360, 2015.
25. Pertea M, Pertea GM, Antonescu CM, Chang TC, Mendell JT and Salzberg SL: StringTie enables improved reconstruction of a transcriptome from RNA-seq reads. Nat Biotechnol 33: 290-295, 2015.
26. Robinson MD, McCarthy DJ and Smyth GK: edgeR: A Bioconductor package for differential expression analysis of digital gene expression data. Bioinformatics 26: 139-140, 2010.
27. Kong L, Zhang Y, Ye ZQ, Liu XQ, Zhao SQ, Wei L and Gao G: CPC: Assess the protein-coding potential of transcripts using sequence features and support vector machine. Nucleic Acids Res 35: W345-W349, 2007.
28. Sun L, Luo H, Bu D, Zhao G, Yu K, Zhang C, Liu Y, Chen R and Zhao Y: Utilizing sequence intrinsic composition to classify protein-coding and long non-coding transcripts. Nucleic Acids Res 41: e166, 2013.
29. Rauluseviciute I, Riudavets-Puig R, Blanc-Mathieu R, Castro-Mondragon JA, Ferenc K, Kumar V, Lemma RB, Lucas J, Chèneby J, Baranasic D, *et al*: JASPAR 2024: 20th anniversary of the open-access database of transcription factor binding profiles. Nucleic Acids Res 52: D174-D182, 2024.
30. Livak KJ and Schmittgen TD: Analysis of relative gene expression data using real-time quantitative PCR and the 2(-Delta Delta C(T)) method. Methods 25: 402-408, 2001.
31. Li MT, Tang XH, Cai H, Zhang AH and Guo ZY: Editorial: Molecular mechanism and therapeutic approach to renal interstitial fibrosis. Front Med (Lausanne) 9: 879927, 2022.
32. Herrera J, Henke CA and Bitterman PB: Extracellular matrix as a driver of progressive fibrosis. J Clin Invest 128: 45-53, 2018.
33. Tan YT, Lin JF, Li T, Li JJ, Xu RH and Ju HQ: LncRNA-mediated posttranslational modifications and reprogramming of energy metabolism in cancer. Cancer Commun (Lond) 41: 109-120, 2021.
34. Robinson EK, Covarrubias S and Carpenter S: The how and why of lncRNA function: An innate immune perspective. Biochim Biophys Acta Gene Regul Mech 1863: 194419, 2020.
35. Slatko BE, Gardner AF and Ausubel FM: Overview of Next-generation sequencing technologies. Curr Protoc Mol Biol 122: e59, 2018.
36. Levy SE and Boone BE: Next-generation sequencing strategies. Cold Spring Harb Perspect Med 9: a025791, 2019.
37. Rego SM and Snyder MP: High throughput sequencing and assessing disease risk. Cold Spring Harb Perspect Med 9: a026849, 2019.
38. Huang D, Chen J, Yang L, Ouyang Q, Li J, Lao L, Zhao J, Liu J, Lu Y, Xing Y, *et al*: NKILA lncRNA promotes tumor immune evasion by sensitizing T cells to activation-induced cell death. Nat Immunol 19: 1112-1125, 2018.
39. Gupta SC, Awasthee N, Rai V, Chava S, Gunda V and Challagundla KB: Long non-coding RNAs and nuclear factor-κB crosstalk in cancer and other human diseases. Biochim Biophys Acta Rev Cancer 1873: 188316, 2020.
40. Liu B, Sun L, Liu Q, Gong C, Yao Y, Lv X, Lin L, Yao H, Su F, Li D, *et al*: A cytoplasmic NF-κB interacting long noncoding RNA blocks IκB phosphorylation and suppresses breast cancer metastasis. Cancer Cell 27: 370-381, 2015.
41. Singh A, Martinez-Yamout MA, Wright PE and Dyson HJ: Interactions of a long noncoding RNA with domains of NF-κB and IκBα: Implications for the inhibition of Non-Signal-related phosphorylation. Biochemistry 61: 367-376, 2022.
42. Gai X and Li L: Overexpression of Long Noncoding RNAs (lncRNA) NF-κβ-interacting long Noncoding RNA (NKILA) in ankylosing spondylitis is correlated with transforming growth factor β1 (TGF-β1), active disease and predicts length of treatment. Med Sci Monit 25: 4244-4249, 2019.
43. Li JP, Li R, Liu X, Huo C, Liu TT, Yao J and Qu YQ: A Seven Immune-related lncRNAs model to increase the predicted value of lung adenocarcinoma. Front Oncol 10: 560779, 2020.
44. Xu G, Yang M, Wang Q, Zhao L, Zhu S, Zhu L, Xu T, Cao R, Li C, Liu Q, *et al*: A novel prognostic prediction model for colorectal cancer based on nine autophagy-Related long noncoding RNAs. Front Oncol 11: 613949, 2021.
45. Jiang P, Han X, Zheng Y, Sui J and Bi W: Long non-coding RNA NKILA serves as a biomarker in the early diagnosis and prognosis of patients with colorectal cancer. Oncol Lett 18: 2109-2117, 2019.
46. Ebadi N, Ghafouri-Fard S, Taheri M, Arsang-Jang S and Omrani MD: Expression analysis of inflammatory response-associated genes in coronary artery disease. Arch Physiol Biochem 128: 601-607, 2022.
47. Liu D and Shi X: Long non-coding RNA NKILA inhibits proliferation and migration of lung cancer via IL-11/STAT3 signaling. Int J Clin Exp Pathol 12: 2595-2603, 2019.
48. He B, Chen W, Zeng J, Tong W and Zheng P: Long noncoding RNA NKILA transferred by astrocyte-derived extracellular vesicles protects against neuronal injury by upregulating NLRX1 through binding to mir-195 in traumatic brain injury. Aging (Albany NY) 13: 8127-8145, 2021.
49. Butturini E, Carcereri de Prati A and Mariotto S: Redox regulation of STAT1 and STAT3 Signaling. Int J Mol Sci 21: 7034, 2020.
50. Butturini E, Boriero D, Carcereri de Prati A and Mariotto S: STAT1 drives M1 microglia activation and neuroinflammation under hypoxia. Arch Biochem Biophys 669: 22-30, 2019.
51. Fu XQ, Chou JY, Li T, Zhu PL, Li JK, Yin CL, Su T, Guo H, Lee KW, Hossen MJ, *et al*: The JAK2/STAT3 pathway is involved in the anti-melanoma effects of atractylenolide I. Exp Dermatol 27: 201-204, 2018.
52. Li R, Sun N, Chen X, Li X, Zhao J, Cheng W, Hua H, Fukatsu M, Mori H, Takahashi H, *et al*: JAK2(V617F) Mutation Promoted IL-6 production and glycolysis via mediating PKM1 stabilization in macrophages. Front Immunol 11: 589048, 2020.
53. Chen WD, Zhang JL, Wang XY, Hu ZW and Qian YB: The JAK2/STAT3 signaling pathway is required for inflammation and cell death induced by cerulein in AR42J cells. Eur Rev Med Pharmacol Sci 23: 1770-1777, 2019.
54. Wang B, Liu T, Wu JC, Luo SZ, Chen R, Lu LG and Xu MY: STAT3 aggravates TGF-β1-induced hepatic epithelial-to-mesenchymal transition and migration. Biomed Pharmacother 98: 214-221, 2018.
55. You X, Jiang X, Zhang C, Jiang K, Zhao X, Guo T, Zhu X, Bao J and Dou H: Dihydroartemisinin attenuates pulmonary inflammation and fibrosis in rats by suppressing JAK2/STAT3 signaling. Aging (Albany NY) 14: 1110-1127, 2022.